Longitudinal momentum distributions of the reaction residues following fast two-nucleon knockout reactions

E. C. Simpson,[1] J. A. Tostevin,[1] D. Bazin,[2] and A. Gade[2,3]

[1]*Department of Physics, Faculty of Engineering and Physical Sciences, University of Surrey, Guildford, Surrey GU2 7XH, United Kingdom*

[2]*National Superconducting Cyclotron Laboratory, Michigan State University, East Lansing, Michigan 48824, USA*

[3]*Department of Physics and Astronomy, Michigan State University, East Lansing, Michigan 48824, USA*

(Received 22 April 2009; published 29 June 2009)

The longitudinal momentum distributions of the cross sections of heavy projectile-like residues after fast, direct two-like-nucleon knockout reactions are discussed. Both the two-nucleon inelastic breakup (stripping) and the stripping-diffraction removal events are considered. We show that, because the two mechanisms have a very similar nuclear surface localization, they generate essentially identical longitudinal momentum distributions. The approach used combines reaction dynamics, using the sudden, eikonal and spectator-core approximations, with structure wave functions from the many-body shell model. The sensitivities of the resulting longitudinal momentum distributions to the orbital angular momenta, the separation energies, and the angular momentum coupling of the two removed nucleons are clarified. In particular, the widths of these distributions are shown to provide a very clear signal of the total angular momentum of the removed-nucleon pair—pairs coupled to larger total angular momentum giving broader distributions. These now complete distributions, from correlated wave functions, are significantly different from earlier uncorrelated estimates. Confirmation of these theoretical expectations is presented, based on very recent intermediate-energy, residue final-state inclusive and exclusive two-nucleon removal measurements.

DOI: 10.1103/PhysRevC.79.064621 PACS number(s): 23.20.Lv, 21.60.Cs, 24.50.+g, 27.30.+t

I. INTRODUCTION

One-nucleon knockout reactions from beams of rare isotopes at intermediate energies, of order 100 MeV/u and greater, have been the subject of study for several years, e.g., Refs. [1–4]. Due in major part to the development and application of coincident γ-ray spectroscopy to the fast reaction residues, permitting final-state exclusive measurements and analyses, including, e.g., Refs. [3,5–11], the reaction is now in routine use for obtaining spectroscopic information on the dominant neutron and proton single-particle configurations near the Fermi surfaces of short-lived isotopes. Experimentally, the potency of the technique arises from (a) the high luminosity associated with the use of thick targets and (b) the high detection efficiency of the forward-traveling projectile-like residues. The observables, the cross sections for populating different residue final states and their distribution with the longitudinal momentum of these residues, derive information on the spectroscopic strength and orbital angular momentum of the removed nucleon, respectively. Analyses have been used to deduce quantitative single-particle spectroscopy in many instances, e.g., Refs. [3,4,12–15], and have contributed significantly to our understanding of the evolution of shell structures in nuclei with the most asymmetric N:Z ratios. Recent examples include Refs. [16–19].

Reactions that remove two like nucleons of an already deficient species, such as occurs in two-proton removal from an already neutron-rich system, involve nucleons that are necessarily well bound. Such reactions, because of the energy thresholds in the one-nucleon removal channels, also proceed as direct (one-step) processes [3,20,21]. These direct reactions have also been described quantitatively using a sudden, eikonal model dynamical description. The calculations include the mechanisms where (a) the two-nucleons are removed by inelastic collisions with the target (stripping) and (b) one of the nucleons is absorbed and the other is diffracted [21,22]. An estimate of the very small direct two-nucleon diffractive breakup contribution was also made [22]. These reactions have been assessed in test regions of the nuclear chart, on well-understood sd-shell nuclei [20,22,23], and are now being used spectroscopically through exclusive measurements of cross sections to the residue final states; see, e.g., Refs. [24–28].

Unlike single-nucleon knockout (and single-nucleon transfer) the cross sections for two-nucleon removal no longer simply factorize into a reaction (single-particle cross section) and a structure (spectroscopic factor) part. The structure input now enters in the form of the initial-state to final-state two-nucleon overlap function, in which the two active (valence) nucleons are correlated and their configurations appear coherently. The sensitivity of two-nucleon knockout reaction yields to these two-nucleon correlations has been discussed in some detail elsewhere [21,23,29,30]. This is not our prime interest here. It is expected, based on the knowledge that the reactions proceed through direct, grazing, and near-surface collisions, that the *shapes* of the longitudinal momentum distributions of the reaction residues will show strong sensitivity to the angular momenta of the removed nucleons and thus to the spins of the final states populated [30,31]. Clarification of the source and level of this sensitivity is the subject of this article.

Therefore, we consider the removal of two nucleons (1, 2) from a projectile of mass $A+2$, incident with momentum $\vec{K}_{A+2}$ in the laboratory frame on a light target (here ^{9}Be). Understanding the observed longitudinal momentum distribution sensitivities is strongly aided by recalling that, in the sudden approximation, event-by-event, the sum of the momenta of the

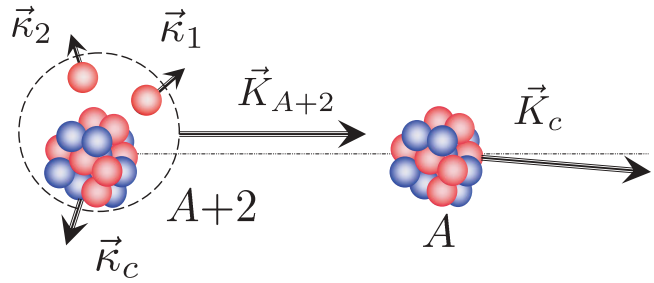

FIG. 1. (Color online) Diagram showing the laboratory momenta of the projectile $\vec{K}_{A+2}$ and the reaction residue $\vec{K}_c$ (the mass A core c). The momenta $\vec{\kappa}_c$, $\vec{\kappa}_1$, and $\vec{\kappa}_2$ are the core and nucleon momenta in the rest frame of the projectile with $\vec{\kappa}_1 + \vec{\kappa}_2 + \vec{\kappa}_c = 0$.

struck/removed nucleons $\vec{\kappa}_1 + \vec{\kappa}_2$ in the projectile's rest frame is probed knowing $\vec{K}_{A+2}$ and the laboratory momentum of the mass A reaction residue (or core of nucleons c), $\vec{K}_c$. Explicitly,

$$\vec{\kappa}_1 + \vec{\kappa}_2 = -\vec{\kappa}_c = \frac{A}{A+2}\vec{K}_{A+2} - \vec{K}_c\,, \tag{1}$$

where $\vec{\kappa}_1 + \vec{\kappa}_2 + \vec{\kappa}_c = 0$ expresses momentum conservation in the projectile rest frame. These quantities are shown schematically in Fig. 1.

The experiments discussed here determine only the longitudinal component of the momentum $\vec{K}_c$, i.e., its component along the direction of the incident beam. We choose this as the z axis of our laboratory and projectile rest frame coordinate systems. Therefore, from this point, we consider only the component of Eq. (1) in the z direction and assume that all symbols, when written as scalars, refer to the z components of these momenta.

There have now been a significant number of such direct two-nucleon removal longitudinal momentum distribution measurements with which to compare model predictions. All of these, however, were inclusive with respect to the bound final states of the residue. We therefore also present results of a reanalysis of the inclusive data of Bazin *et al.* [20], with the largest inclusive two-proton removal cross section yet measured, from which exclusive distributions for two final states with different spins J_f have been extracted.

The present article develops the formalism of Refs. [21] and [22] to include calculations of the differential two-nucleon removal cross section with respect to the longitudinal momentum of the residues, κ_c and K_c. The formalism for the stripping of the two nucleons is developed in Sec. II. Section III first looks at the surface localization of reaction mechanism and then at the sensitivity of the calculated stripping momentum distributions to (a) the total angular momentum and the projection (I, μ) of the removed nucleon pair and (b) the assumed two-nucleon separation energy. Comparison of these new results with earlier and simpler uncorrelated calculations are also presented. The formalism of Sec. II is then exploited to calculate the momentum distributions of the diffraction-stripping terms approximately, but to a sufficient accuracy to demonstrate the strong similarity of their shapes with those of the stripping terms.

In Sec. IV we apply the formalism to three direct, two-like-nucleon knockout reactions for which recent data are available. These are ^{22}Mg$(-2n)$ at 75 MeV/u, involving a neutron-deficient projectile, ^{38}Si$(-2p)$ at 83 MeV/u, and ^{28}Mg$(-2p)$ at 82 MeV/u, the latter two involving neutron-rich projectiles. The last of these presents the reanalysis of the hitherto inclusive longitudinal momentum distribution data of Ref. [20] for the exclusive $J_f^\pi = 0_1^+$ and 4_1^+ state distributions. A short report of these cases was presented in Ref. [31]. Finally, we consider the implications of our formalism for heavier nuclei, taking as an example two-proton knockout from ^{208}Pb. We present the momentum distributions resulting from the removal of two $\pi[0h_{11/2}]$ protons. The strong dependence of the heavy residue momentum distribution on the final-state spin J_f and its magnetic substates is shown to persist, each final state having a very different residue momentum distribution.

II. FORMALISM

We discuss two-nucleon knockout from a secondary projectile beam. We now develop the formalism for the distribution of the cross section with the longitudinal momentum κ_c of the reaction residue in the projectile rest frame. This must be translated to the laboratory frame, applying the appropriate Lorentz boost and convolutions with the experimental resolutions, prior to comparison with experiment.

As much as is possible, we adhere to the notations developed in Refs. [21] and [22]. The projectile is described by an antisymmetrized $A + 2$-body wave function, denoted by $\Psi_{J_i M_i}(A, 1, 2)$, with spin J_i and projection M_i. The position vectors of the initially bound nucleons 1 and 2 relative to the center-of-mass of the core of nucleons are $\vec{r}_i$, and their cylindrical polar coordinates are written as $(\vec{s}_i, z_i) \equiv (s_i, \varphi_i, z_i)$. Recoil effects associated with the heavy, mass A core are neglected. The impact parameters of the center-of-mass of the projectile and the core, $\vec{b} \equiv (b, \varphi)$, are therefore taken to coincide. The individual nucleon impact parameters with the target are thus $\vec{b}_i = \vec{b} + \vec{s}_i$. This coordinate set is presented in Fig. 2.

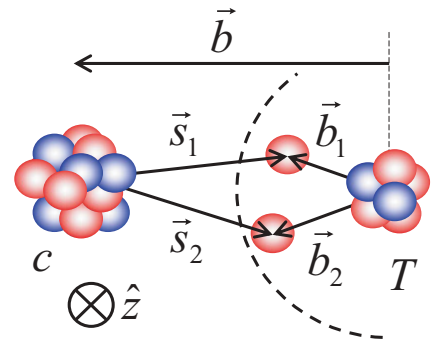

FIG. 2. (Color online) The particle coordinates used in this article. The vectors $\vec{s}_i$ are the components, in the plane perpendicular to the beam direction (the z axis), of the position vectors $\vec{r}_i$ of the knocked-out nucleons relative to the core of nucleons to which they are initially bound. The two nucleons have impact parameters $\vec{b}_i = \vec{b} + \vec{s}_i$ relative to the target nucleus. The target T overlaps the wave function of the two nucleons at and near the surface of the projectile.

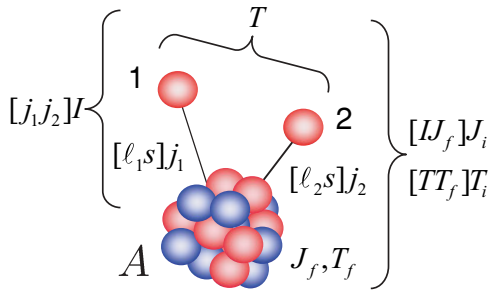

FIG. 3. (Color online) Schematic of the angular momentum and isospin coupling schemes used here for the two-nucleon knockout reaction.

A. Two-nucleon overlap wave function

We first discuss the all-important two-nucleon wave function probed in the reaction. The two nucleons (1,2) will be removed by stripping (absorption) or diffractive dissociation from a set of active (and in general partially occupied) single-particle orbitals ϕ_j, e.g., selected sd-shell and/or pf-shell orbitals in most of the cases of recent interest. These orbitals are assumed to have spherical (shell model) single-particle quantum numbers $n(\ell s)j, m$. The angular momentum and isospin coupling schemes used are discussed in Refs. [21] and [22] and are summarized in the Fig. 3. Specifically, the two removed nucleons couple to an intermediate total angular momentum I, with projection μ, and total isospin T, with projection τ.

We assume throughout, consistent with the sudden approximation, that the internal states of the mass A projectile core are unchanged throughout the reaction—the spectator-core approximation. That is, there is no dynamical coupling of the A-body core states. So, the population of a given physical low-lying final-state f of the residue, with spin J_f, will proceed through the amplitude for finding this core configuration (plus two nucleons) in the projectile ground state (g.s.). We denote by $F \equiv (f, M_f)$ the A-body final state, with wave function $\Phi_{J_f M_f}(A)$, in a particular magnetic substate. This notation elaborates that of Ref. [21]. A transition to state F will therefore probe the (two-nucleon) overlap function of the projectile and residue states, denoted $\Psi^{(F)}_{J_i M_i}(1,2)$, where

$$\Psi^{(F)}_{J_i M_i} \equiv \langle \Phi_{J_f M_f}(A) | \Psi_{J_i M_i}(A,1,2) \rangle = \sum_{I\mu\alpha} C_\alpha^{J_i J_f I} (I\mu J_f M_f | J_i M_i) [\overline{\phi_{j_1} \otimes \phi_{j_2}}]_{I\mu}, \quad (2)$$

and the coefficients $C_\alpha^{J_i J_f I}$ are the two-nucleon amplitudes (TNA). These will be taken from shell-model calculations. The index α identifies the quantum number set of a given two-nucleon configuration, that is, $\alpha \equiv (n_1 \ell_1 j_1, n_2 \ell_2 j_2) \equiv (\beta_1, \beta_2)$, while β is used to label an individual orbital. In the overlap, the antisymmetrized wave functions of the two nucleons are

$$[\overline{\phi_{j_1} \otimes \phi_{j_2}}]_{I\mu} = D_\alpha \sum_{m_1 m_2} (j_1 m_1 j_2 m_2 | I\mu) \times \left[\phi^{m_1}_{j_1}(1)\phi^{m_2}_{j_2}(2) - \phi^{m_1}_{j_1}(2)\phi^{m_2}_{j_2}(1)\right], \quad (3)$$

where $D_\alpha = 1/\sqrt{2(1+\delta_{\beta_1\beta_2})}$. These expressions neglect explicit isospin labels for simplicity, but isospin is included as in Ref. [21]. The above formalism can be used for like-nucleon knockout with TNA calculated in isospin ($T = 1$) or proton-neutron format. Unlike-pair knockout (np removal) is not discussed here.

B. Eikonal reaction dynamics

The second required ingredient is the eikonal reaction dynamics. The absorptive and refractive (optical) interactions of the two nucleons (1,2) and the core of nucleons with the target nucleus are described via their elastic S matrices, $\mathcal{S}_i(b_i)$ ($i = 1, 2, f$), functions of their respective impact parameters. We assume these have no explicit spin dependence. The spectator-core assumption has been discussed already. It is also assumed that the interaction of the core/residue with the target is the same for all low-lying final states $\Phi_{J_f M_f}(A)$. Thus, $\mathcal{S}_f(b)$ is assumed to be both diagonal in the core final states and f independent. All $\mathcal{S}_f$ are replaced by $\mathcal{S}_c$, calculated from the residue ground state density; so

$$\langle \Phi_{J'_f M'_f} | \mathcal{S}_f | \Phi_{J_f M_f} \rangle = \mathcal{S}_c(b)\, \delta_{ff'} \delta_{J_f J'_f} \delta_{M_f M'_f}. \quad (4)$$

In this limit, the total projectile-target absorption cross section is given by the projectile ground state expectation value of the reaction absorption probability, integrated over center-of-mass impact parameters

$$\sigma_{\rm abs} = \frac{1}{\hat{J}_i^{\,2}} \sum_{M_i} \int d\vec{b} \langle \Psi_{J_i M_i} | [1 - |\mathcal{S}_c \mathcal{S}_1 \mathcal{S}_2|^2] | \Psi_{J_i M_i} \rangle. \quad (5)$$

On expanding the absorption operators, using $1 = \prod_{i=1,2,c}\{[1-|\mathcal{S}_i|^2] + |\mathcal{S}_i|^2\}$, and retaining only those terms where the core is not absorbed by the target, i.e., the $|\mathcal{S}_c|^2$ terms, the contributions to the absorption cross section from events in which two nucleons and one nucleon interact inelastically with the target involve the operators

$$\mathcal{O}_{\rm str}(c,1,2) = |\mathcal{S}_c|^2 \mathcal{K}_1(1,2), \quad (6)$$

$$\mathcal{O}_{\rm ds}(c,1,2) = |\mathcal{S}_c|^2 \mathcal{K}_2(1,2), \quad (7)$$

respectively. The $\mathcal{K}_1$ and $\mathcal{K}_2$ are the combinations [22]

$$\mathcal{K}_1(1,2) = (1-|\mathcal{S}_1|^2)(1-|\mathcal{S}_2|^2) \quad (8)$$

$$\mathcal{K}_2(1,2) = |\mathcal{S}_1|^2(1-|\mathcal{S}_2|^2) + (1-|\mathcal{S}_1|^2)|\mathcal{S}_2|^2. \quad (9)$$

The operator $\mathcal{O}_{\rm str}$, involving the joint probability for the absorption of both nucleons, describes stripping (inelastic breakup) and was detailed in Ref. [21]. The total two-nucleon stripping (absorption) cross section is therefore

$$\sigma_{\rm str} = \frac{1}{\hat{J}_i^{\,2}} \sum_{M_i} \int d\vec{b} \langle \Psi_{J_i M_i} | \mathcal{O}_{\rm str}(c,1,2) | \Psi_{J_i M_i} \rangle. \quad (10)$$

As it stands, the second term, $\mathcal{O}_{\rm ds}(c,1,2)$ of Eq. (7), describes the joint probability for absorption of one nucleon and an elastic interaction of the second with the target. It requires modification, by projection-off bound state orbitals, to correctly describe the elastic dissociation of the second nucleon, as was discussed in Ref. [22]. Thus corrected, the

diffraction-stripping (ds) operator reads

$$\mathcal{O}_{\rm ds}(c,1,2) = |\mathcal{S}_c|^2[\mathcal{K}_2(1,2) - \mathcal{K}_3(1,2)], \tag{11}$$

where $\mathcal{K}_3$, which treats the projection-off nucleon bound states, is

$$\mathcal{K}_3(1,2) = \sum_{j''m''} \left[\mathcal{S}_1^* \left|\phi_{j''}^{m''}\right\rangle\left\langle\phi_{j''}^{m''}\right| \mathcal{S}_1(1-|\mathcal{S}_2|^2) + (1-|\mathcal{S}_1|^2)\mathcal{S}_2^* \left|\phi_{j''}^{m''}\right\rangle\left\langle\phi_{j''}^{m''}\right| \mathcal{S}_2\right]. \tag{12}$$

Previously, the sum on j'' was taken over all the active orbitals near the removed particle's Fermi surface [22].

In the following we derive explicitly the momentum distribution arising from an operator with the (product) structure of the stripping term of Eqs. (6) and (8). We then show that the important diffraction-stripping contributions, from $\mathcal{O}_{\rm ds}(c,1,2)$ of Eq. (11), can be approximated and that, as is expected from the similar surface localization of the two reaction mechanisms, their resulting momentum distributions are essentially identical. This will be discussed further in Sec. III E. The total two-nucleon knockout operator is, of course,

$$\mathcal{O}_{\rm ko}(c,1,2) = \mathcal{O}_{\rm str} + \mathcal{O}_{\rm ds}. \tag{13}$$

C. Wave function and momentum sampling

Having made the assumptions that (a) the core is a spectator and (b) its S matrix is both f independent and diagonal in the core states, we can now integrate out explicit consideration of the internal degrees of freedom of the core; thus,

$$\left\langle \Psi_{J_iM_i}\middle|\Psi_{J_iM_i}\right\rangle_A = \sum_f \left[\sum_{M_f} \left|\Psi^{(F)}_{J_iM_i}(1,2)\right|^2\right]. \tag{14}$$

The cross section is thus the sum of contributions from each core state f, $\sigma_{\rm str} = \sum_f \sigma_{\rm str}^{(f)}$, and the exclusive stripping cross sections are

$$\sigma_{\rm str}^{(f)} = \frac{1}{\hat{J}_i^{\,2}} \sum_{M_iM_f} \int d\vec{b} \left\langle \Psi^{(F)}_{J_iM_i}\middle|\mathcal{O}_{\rm str}(c,1,2)\middle|\Psi^{(F)}_{J_iM_i}\right\rangle. \tag{15}$$

Further, because $\mathcal{O}_{\rm str}$ depends only on impact parameters, we can also take it outside the integral over the nucleon z coordinates and write these cross sections as

$$\sigma_{\rm str}^{(f)} = \int d\vec{b} \int d\vec{s}_1 \int d\vec{s}_2\, \mathcal{P}_f(\vec{s}_1,\vec{s}_2)\mathcal{O}_{\rm str}(c,1,2), \tag{16}$$

where, having summed over the nucleon intrinsic spin coordinates, $\mathcal{P}_f(\vec{s}_1,\vec{s}_2)$ is the joint position probability for finding the nucleons with position projections $\vec{s}_1$ and $\vec{s}_2$ on the plane normal to the beam direction. That is,

$$\mathcal{P}_f(\vec{s}_1,\vec{s}_2) = \frac{1}{\hat{J}_i^{\,2}} \sum_{M_iM_f} \int dz_1 \int dz_2 \left\langle \left|\Psi^{(F)}_{J_iM_i}\right|^2\right\rangle_{\rm sp}. \tag{17}$$

In this form, the dependence of the removal cross sections on the (essentially geometrical) two-nucleon stripping reaction joint probability $\mathcal{O}_{\rm str}$ and the structure-driven, correlated-nucleon joint position probabilities $\mathcal{P}_f$ is particularly transparent.

We can now discuss the residue longitudinal momentum distributions $d\sigma_{\rm str}^{(f)}/d\kappa_c$. While the spatial stripping reaction sampling $\mathcal{O}_{\rm str}$ remains unchanged, we now need the differential two-nucleon joint position probability for each value of the sum of their momenta, that is, the residue momentum $\kappa_c = -[\kappa_1+\kappa_2]$; see Fig. 1 and Eq. (1). This is obtained by taking the Fourier transform of the two-nucleon wave function with respect to each nucleon z coordinate, with the constraint that $\kappa_c + \kappa_1 + \kappa_2 = 0$. This differential joint position probability distribution with κ_c is

$$\bar{\mathcal{P}}_f(\vec{s}_1,\vec{s}_2,\kappa_c) = \frac{1}{\hat{J}_i^{\,2}} \sum_{M_iM_f} \int d\kappa_1 \int d\kappa_2 \frac{\delta(\kappa_c+\kappa_1+\kappa_2)}{(2\pi)^2} \times \left\langle \left| \int dz_1 \int dz_2 e^{i\kappa_1 z_1} e^{i\kappa_2 z_2} \Psi^{(F)}_{J_iM_i} \right|^2 \right\rangle_{\rm sp}, \tag{18}$$

and the final-state exclusive longitudinal momentum distribution is

$$\frac{d\sigma_{\rm str}^{(f)}}{d\kappa_c} = \int d\vec{b} \int d\vec{s}_1 \int d\vec{s}_2\, \bar{\mathcal{P}}_f(\vec{s}_1,\vec{s}_2,\kappa_c)\mathcal{O}_{\rm str}(c,1,2). \tag{19}$$

Thus, both the total and differential stripping cross sections are determined by the two-nucleon overlap functions and their momentum content within a volume, extending along the z direction. Its position, near the nuclear surface, and constant cross-sectional area are determined by the eikonal two-nucleon absorption and core survival joint probability factor $\mathcal{O}_{\rm str}(c,1,2)$.

Inspection of Eqs. (6), (8), and (19) shows that the reaction will be strongly localized in the impact parameter b when knocking out well-bound nucleons. So, if the $\bar{\mathcal{P}}_f$ do not change rapidly with the nucleon positions over the (relatively small) range of $\vec{s}_i$ values sampled by the target, the shapes of the $d\sigma_{\rm str}^{(f)}/d\kappa_c$ distributions can be estimated simply from those of the $\bar{\mathcal{P}}_f$ at fixed nucleon positions near the projectile surface. This scheme formed the basis of an earlier short communication [30]. Equation (19) is calculated fully in this work, but the results show that this earlier estimate provides a rather accurate description of these shapes. This shows, at a fundamental level, that the shapes of the longitudinal momentum distributions are extremely robust and stem from the geometrical selectivity of the reaction mechanisms. It is for this reason that the stripping and the diffraction-stripping mechanisms lead to very similar distributions, as is shown later.

While very transparent, revealing the physical content and the spatial sampling of the wave functions by the reaction mechanism, for effective computation the above formula, must be restructured to take advantage of separations of the nucleon variables within the multidimensional integral whenever possible. This angular momentum and coordinate decomposition is carried out in the next subsection.

D. Reduction of the stripping term

It is convenient to revert to Eq. (15) for the exclusive stripping cross section that we now write as

$$\sigma_{\rm str}^{(f)} = \frac{1}{\hat{j}_i^{\,2}} \sum_{M_i M_f} \int d\vec{b} |\mathcal{S}_c|^2 \langle \Psi^{(F)}_{J_i M_i} | \mathcal{K}_1(1,2) | \Psi^{(F)}_{J_i M_i} \rangle, \quad (20)$$

and where the bra-ket denotes integration over the position coordinates $\vec{r}_1$ and $\vec{r}_2$ of the nucleons and their intrinsic spins. Because the nucleon S matrices and $\mathcal{K}_1$ are spin independent we require only the spin-integrated two-nucleon wave function. We extract the nucleon position integrals explicitly and write

$$\langle \Psi^{(F)}_{J_i M_i} | \cdots | \Psi^{(F)}_{J_i M_i} \rangle = \int d\vec{r}_1 \int d\vec{r}_2 \langle \Psi^{(F)}_{J_i M_i} | \cdots | \Psi^{(F)}_{J_i M_i} \rangle_{\rm sp}. \quad (21)$$

Upon substituting our antisymmetrized two-nucleon wave functions from Eqs. (2) and (3), this gives a sum of contributions, incoherent with respect to different values of the two-nucleon total angular momentum I, but coherent in the two-nucleon configurations α, α' to each final state f, that is,

$$\begin{aligned}
&\frac{1}{\hat{j}_i^{\,2}} \sum_{M_i M_f} \langle \Psi^{(F)}_{J_i M_i} | \Psi^{(F)}_{J_i M_i} \rangle_{\rm sp} \\
&= \sum_{\alpha\alpha' I} \frac{C^{J_i J_f I}_{\alpha'} C^{J_i J_f I}_{\alpha} D_{\alpha'} D_{\alpha}}{\hat{I}^2} \\
&\quad \times \sum_{m_1 m_2 m_1' m_2' \mu} (j_1 m_1 j_2 m_2 | I\mu)(j_1' m_1' j_2' m_2' | I\mu) \\
&\quad \times \Big[\big(\phi^{m_1'}_{j_1'} | \phi^{m_1}_{j_1}\big)_{\rm sp} \big(\phi^{m_2'}_{j_2'} | \phi^{m_2}_{j_2}\big)_{\rm sp} + \big(\phi^{m_2'}_{j_2'} | \phi^{m_2}_{j_2}\big)_{\rm sp} \big(\phi^{m_1'}_{j_1'} | \phi^{m_1}_{j_1}\big)_{\rm sp} \\
&\quad - \big(\phi^{m_1'}_{j_1'} | \phi^{m_2}_{j_2}\big)_{\rm sp} \big(\phi^{m_2'}_{j_2'} | \phi^{m_1}_{j_1}\big)_{\rm sp} - \big(\phi^{m_2'}_{j_2'} | \phi^{m_1}_{j_1}\big)_{\rm sp} \big(\phi^{m_1'}_{j_1'} | \phi^{m_2}_{j_2}\big)_{\rm sp} \Big].
\end{aligned} \quad (22)$$

We refer to the first two terms of the sum in the square bracketed part of Eq. (22) as the *direct* terms and the final two as the *exchange* terms. For each product of brackets, $(\,|\,)_{\rm sp}(\,|\,)_{\rm sp}$, the first bracket takes the coordinates of nucleon 1 and the second bracket those of nucleon 2. Each individual bracket involves the product of two single-particle orbitals and the notation (sp) indicates that these products are summed over the spin coordinate for that nucleon. These are written

$$\begin{aligned}
\big(\phi^{m'}_{j'} | \phi^{m}_{j}\big)_{\rm sp} &= \sum_{\lambda\lambda'\sigma} (\ell\lambda s\sigma | jm)(\ell'\lambda' s\sigma | j'm') \\
&\quad \times \big[\mathcal{C}_{\ell\lambda} u_{j\ell}(r) P_\ell^{|\lambda|}(\cos\theta)\big] \\
&\quad \times \big[\mathcal{C}_{\ell'\lambda'} u_{j'\ell'}(r) P_{\ell'}^{|\lambda'|}(\cos\theta)\big]^* \\
&\quad \times \exp[i(\lambda - \lambda')\varphi],
\end{aligned} \quad (23)$$

where the $u_{j\ell}(r)$ are the nucleon single-particle radial wave functions and θ is the spherical polar angle of $\vec{r}$. The $\mathcal{C}_{\ell\lambda}$ are the spherical harmonic constants of Ref. [32],

$$\mathcal{C}_{\ell\lambda} = (-1)^\lambda \left[\frac{(2\ell+1)}{4\pi} \frac{(\ell-\lambda)!}{(\ell+\lambda)!} \right]^{1/2}, \quad (24)$$

for $\lambda \geqslant 0$, and $\mathcal{C}_{\ell\lambda} = (-1)^\lambda \mathcal{C}_{\ell|\lambda|}$ for $\lambda < 0$.

To now obtain the longitudinal momentum distribution we insert the following unit operator appropriately in each of the two nucleon coordinates, i.e.,

$$\frac{1}{2\pi} \int dz' \int d\kappa \exp[i\kappa(z'-z)] = 1, \quad (25)$$

with κ the momentum (wave number) of the nucleon in the beam (z) direction. Thus, when combining Eq. (22) and Eq. (21) and with $\mathcal{K}_1(1,2)$ of Eq. (20) we obtain the following integral in each nucleon coordinate,

$$\begin{aligned}
\mathcal{I}_i &= \frac{1}{2\pi} \int d\vec{r}_i (1 - |\mathcal{S}_i|^2) \\
&\quad \times \big(\phi^{m'}_{j'} \big| \int d\kappa_i \int dz_i' \exp[i\kappa_i(z_i' - z_i)] \big| \phi^{m}_{j}\big)_{\rm sp}.
\end{aligned} \quad (26)$$

This integral, reexpressed using the nucleon's cylindrical polar coordinates (s_i, φ_i, z_i) can be written as the integral of the product of three one-variable integrals,

$$\mathcal{I}_i = \int d\kappa_i \int ds_i s_i \, \mathcal{H}_{\lambda\lambda'}(i) \, \mathcal{R}^{j}_{\ell\lambda}(i) \, \mathcal{R}^{*j'}_{\ell'\lambda'}(i), \quad (27)$$

where we have defined the function $\mathcal{R}^{j}_{\ell\lambda}(i) \equiv \mathcal{R}^{j}_{\ell\lambda}(s_i, \kappa_i)$ for the integral over z_i,

$$\mathcal{R}^{j}_{\ell\lambda}(i) = \frac{\mathcal{C}_{\ell\lambda}}{\sqrt{2\pi}} \int_{-\infty}^{\infty} dz_i u_{j\ell}(r_i) P_\ell^{|\lambda|}(\cos\theta_i) \exp[-i\kappa_i z_i], \quad (28)$$

and $\mathcal{H}_{\lambda\lambda'}(i) \equiv \mathcal{H}_{\lambda\lambda'}(b, s_i)$ for the integral over φ_i,

$$\mathcal{H}_{\lambda\lambda'}(i) = \int_0^{2\pi} d\varphi_i (1 - |\mathcal{S}_i(b_i)|^2) \exp[i\varphi_i(\lambda - \lambda')]. \quad (29)$$

Here b is the common impact parameter of the projectile center-of-mass and the reaction residue.

When not considering the momentum distribution [21,22] it was possible to sum over all angular momentum projections except one. In particular, the two spherical harmonics for each nucleon, originating from the nucleon wave functions ϕ_j, could be recoupled. The necessity here to factorize the integrals, through the functions $\mathcal{H}$ and $\mathcal{R}$, results in explicit dependencies on the λ, but we may now sum over all other projections. We write down only the first direct term in Eq. (22). All other terms are related to this by an appropriate permutation of orbital or particle labels and a resulting phase. This term brings six Clebsch-Gordan coefficients and, with $\beta_i \equiv n_i \ell_i j_i$,

$$\begin{aligned}
\mathcal{G}^{\beta_1\beta_2\beta_1'\beta_2' I}_{\lambda_1\lambda_2\lambda_1'\lambda_2'} &= \sum_{\substack{m_1 m_1' m_2 m_2' \\ \sigma_1\sigma_2\mu}} (j_1 m_1 j_2 m_2 | I\mu)(j_1' m_1' j_2' m_2' | I\mu) \\
&\quad \times (\ell_1\lambda_1 s\sigma_1 | j_1 m_1)(\ell_1'\lambda_1' s\sigma_1 | j_1' m_1') \\
&\quad \times (\ell_2\lambda_2 s\sigma_2 | j_2 m_2)(\ell_2'\lambda_2' s\sigma_2 | j_2' m_2'),
\end{aligned} \quad (30)$$

which can be recoupled to

$$\mathcal{G}^{\beta_1\beta_2\beta_1'\beta_2' I}_{\lambda_1\lambda_2\lambda_1'\lambda_2'} = (-)^{\ell_1+\ell_2+j_1+j_2-2s}\,\frac{\hat{j}_1\hat{j}_1'\hat{j}_2\hat{j}_2'\hat{I}^2}{\hat{\ell}_1'\hat{\ell}_2'} \times \sum_{kq}(-)^{k+q}\,\hat{k}^2\,(\ell_1\lambda_1 kq|\ell_1'\lambda_1') \times (\ell_2\lambda_2 k-q|\ell_2'\lambda_2')W(j_1\ell_1 j_1'\ell_1';sk) \times W(j_2\ell_2 j_2'\ell_2';sk)W(j_2 I k j_1';j_1 j_2'). \quad (31)$$

Finally, the stripping cross section, differential with respect to the residue momentum κ_c, is

$$\frac{d\sigma^{(f)}_{\rm str}}{d\kappa_c} = \int d\kappa_1 \int d\kappa_2\,\delta(\kappa_1+\kappa_2+\kappa_c)\int d\vec{b}|\mathcal{S}_c(b)|^2 \times \sum_{I\alpha\alpha'}\frac{C^{J_iJ_fI}_{\alpha'}C^{J_iJ_fI}_{\alpha}D_{\alpha'}D_{\alpha}}{\hat{I}^2} \times \sum_{\lambda_1\lambda_2\lambda_1'\lambda_2'}\int ds_1 s_1\int ds_2 s_2[\text{direct}-\text{exchange}], \quad (32)$$

where the *direct* and *exchange* terms are

$$\text{direct} = \mathcal{G}^{\beta_1\beta_2\beta_1'\beta_2' I}_{\lambda_1\lambda_2\lambda_1'\lambda_2'}\{\mathcal{H}_{\lambda_1\lambda_1'}(1)\mathcal{H}_{\lambda_2\lambda_2'}(2)\mathcal{R}^{j_1}_{\ell_1\lambda_1}(1)\mathcal{R}^{*j_1'}_{\ell_1'\lambda_1'}(1) \times \mathcal{R}^{j_2}_{\ell_2\lambda_2}(2)\mathcal{R}^{*j_2'}_{\ell_2'\lambda_2'}(2)+\mathcal{H}_{\lambda_1\lambda_1'}(2)\mathcal{H}_{\lambda_2\lambda_2'}(1) \times \mathcal{R}^{j_1}_{\ell_1\lambda_1}(2)\mathcal{R}^{*j_1'}_{\ell_1'\lambda_1'}(2)\mathcal{R}^{j_2}_{\ell_2\lambda_2}(1)\mathcal{R}^{*j_2'}_{\ell_2'\lambda_2'}(1)\}, \quad (33)$$

$$\text{exchange} = (-)^{j_1+j_2-I}\mathcal{G}^{\beta_2\beta_1\beta_1'\beta_2' I}_{\lambda_2\lambda_1\lambda_1'\lambda_2'}\{\mathcal{H}_{\lambda_2\lambda_1'}(1)\mathcal{H}_{\lambda_1\lambda_2'}(2)\mathcal{R}^{j_2}_{\ell_2\lambda_2}(1) \times \mathcal{R}^{*j_1'}_{\ell_1'\lambda_1'}(1)\mathcal{R}^{j_1}_{\ell_1\lambda_1}(2)\mathcal{R}^{*j_2'}_{\ell_2'\lambda_2'}(2)+\mathcal{H}_{\lambda_2\lambda_2'}(2)\mathcal{H}_{\lambda_1\lambda_2'}(1) \times \mathcal{R}^{j_2}_{\ell_2\lambda_2}(2)\mathcal{R}^{*j_1'}_{\ell_1'\lambda_1'}(2)\mathcal{R}^{j_1}_{\ell_1\lambda_1}(1)\mathcal{R}^{*j_2'}_{\ell_2'\lambda_2'}(1)\}. \quad (34)$$

In this highly factored form the differential cross-section calculation is rather efficient. Before we discuss our treatment of the diffraction-stripping term, from $\mathcal{O}_{\rm ds}(c,1,2)$, and compare with experiment, we discuss the general results and sensitivities arising from this stripping mechanism.

III. MOMENTUM DISTRIBUTION SENSITIVITIES

We first discuss initial results for calculated longitudinal momentum distributions resulting from this stripping formalism, showing the general trends and the sensitivities to physical parameters. In the case of even-even $J_i^\pi = 0^+$ projectile nuclei, the spin and projections J_f, M_f of the residue final state are uniquely fixed by the total angular momentum of the removed pair of nucleons, I, μ, with $J_f = I, M_f = -\mu$. There is thus a very direct and clear connection between the residue final state populated and the corresponding two-nucleon overlap.

In this section we make use of a simplified model of pure $\pi[0d_{5/2}]^2$ two-proton stripping from the ^{28}Mg(0^+) ground state at 82 MeV/u. Identical proton radial wave functions are used in each calculation. We look first at the spatial localization of the reaction.

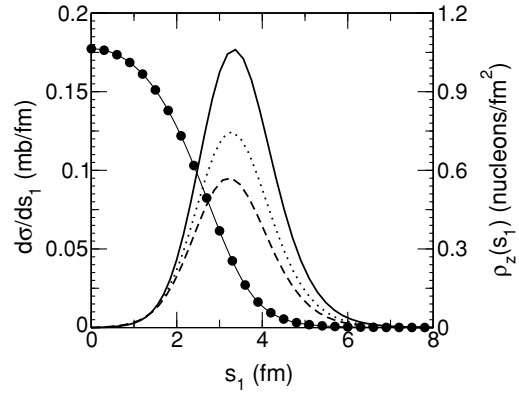

FIG. 4. The differential stripping cross section with respect to s_1, the component of the nucleon position vector in the plane perpendicular to the beam direction. The calculation is for $\pi[0d_{5/2}]^2$ two-proton removal from ^{28}Mg at 82 MeV/u. The localization for $I^\pi = 0^+$ (solid), 2^+ (dotted), and 4^+ (dashed) states are shown, the peak moving marginally inward as I increases. Also shown is the associated z-integrated ^{26}Ne core density as a function of the radial distance s_1 (symbols).

A. Surface localization

Understanding the surface localization of the reaction is important both intuitively and to provide information on those parts of the wave function probed by the knockout mechanism. So, we first consider the contributions to the partial knockout cross sections as a function of a nucleon's position s_1 in the impact parameter plane (see Fig. 2). This is shown in Fig. 4 for the $I^\pi = 0^+$, 2^+, and 4^+ ^{26}Ne final-state transitions. The surface localization is clear, the important s_1 being in the range 2 to 5 fm, near the surface of the ^{26}Ne core.

The near-surface and nonasymptotic nature of this localization is important for the reaction's spectroscopic sensitivity. Conversely, the reaction calculations need a realistic description both of the size of the active single-particle orbitals and of their surface behavior. In the following these requirements are assisted by constraining the single-particle wave functions for different systems using Hartree-Fock systematics.

B. Sensitivity to the two-nucleon coupling

Next we will show (a) that it is the total two-proton angular momentum I that principally determines the shape of the residue longitudinal momentum distribution and (b) that the larger I lead to broader distributions. This key result is shown in Fig. 5. We can label the final state distributions by I, μ, as discussed above, and the increasing width of the distributions with I is very evident.

These features can be understood semiclassically. The $I^\pi = 0^+$ configuration involves the coupling of time-reversed orbitals for which the summed nucleon momenta are small, in any direction. This is reflected in the narrow longitudinal distribution shown (solid curve). For comparison, Fig. 5 also shows (solid line with open circles) the corresponding $\pi[0d_{5/2}]$ one-proton knockout distribution for the same one-proton separation energy. This is considerably broader than the $I^\pi = 0^+$ two-proton distribution, showing that it is the correlated

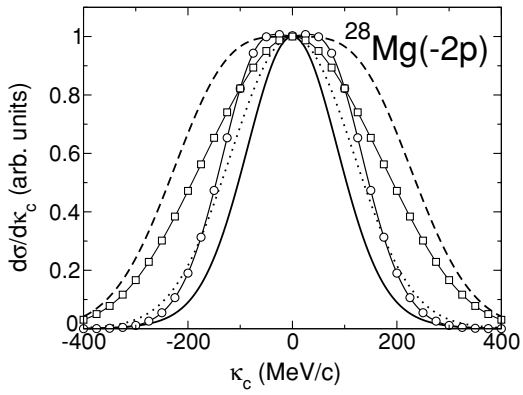

FIG. 5. The variation of the stripping longitudinal momentum distribution with I for $\pi[0d_{5/2}]^2$ two-proton removal from ^{28}Mg at 82 MeV/u. The curves are for $I^\pi = 0^+$ (solid), 2^+ (dotted), and 4^+ (dashed). The solid line with open circles shows the corresponding $\pi[0d_{5/2}]$ one-proton knockout distribution for the same single-particle orbital and separation energy, which is significantly wider than the $I^\pi = 0^+$ two-proton distribution. The solid line with open squares shows the distribution from removal of two uncorrelated protons, discussed in Sec. III C. All distributions have been normalized to the same peak value.

time-reversed motions of the two protons that reduce the κ_c in this configuration. The $I^\pi = 4^+$ configuration, however, requires the two protons to have near-aligned j and, for small μ, will result in large summed nucleon momenta parallel and antiparallel to the beam direction; hence the broad distribution of κ_c in this configuration. Thus, for each nucleon pair coupling the longitudinal momentum distribution will vary sensitively with I and for $I > 0$ with its projection $|\mu|$. With increasing $|\mu|$, and increasing alignment of I with the beam direction, the nucleon pair will orbit preferentially in the plane perpendicular to the beam direction, with small longitudinal momentum components. Figure 6 shows the momentum distributions as

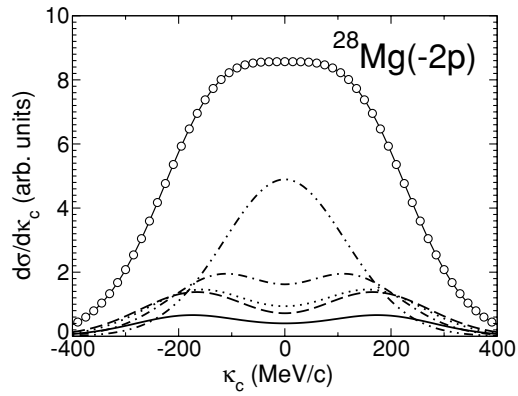

FIG. 6. The sensitivity of the calculated stripping longitudinal momentum distributions to $|\mu|$ for $\pi[0d_{5/2}]^2$ two-proton removal from ^{28}Mg at 82 MeV/u. The cases of $I^\pi = 4^+$ with $|\mu| = 0$ (solid), 1 (dashed), 2 (dotted), 3 (dot-dashed), and 4 (dot-dot-dashed) are shown. The solid curve with open circles is the $I^\pi = 4^+$ distribution summed over all μ, as is shown in Fig. 5. The variation with $|\mu|$ is clear, the narrower distributions arising from the largest projections (see text).

a function of $|\mu|$ for $I^\pi = 4^+$. The expected narrowing of the distributions with increasing $|\mu|$ is evident, with $|\mu| = 4$ producing the narrowest distribution. It is expected, therefore, that the $|\mu| = I$ distribution will also become narrower with increasing I.

C. Uncorrelated two-nucleon knockout

In Ref. [21], two-nucleon removal cross sections were calculated assuming wave functions that were both fully correlated, the antisymmetrized, angular momentum coupled, pair wave functions of Eq. (2), and completely uncorrelated, with two nucleons moving independently about a common core. There it was clear that the I-dependent pair correlations, built into the joint position probabilities $\mathcal{P}_f$ of Eq. (17) by the correlated wave functions, are vital to obtain the correct partial cross sections from Eq. (16). We can also calculate the (now I-independent) two-nucleon removal momentum distribution for uncorrelated nucleons using our $\pi[0d_{5/2}]^2$, ^{28}Mg(0^+) example. This distribution is, to a good approximation, the convolution of two independent $\pi[0d_{5/2}]$ one-proton knockout momentum distributions. This model was used as a first assessment of the inclusive longitudinal momentum of ^{26}Ne residues in Ref. [20].

The uncorrelated cross section for stripping two nucleons, one from each of the orbitals j_1 and j_2, is

$$\sigma^{\rm unc}_{j_1 j_2} = \int d\vec{b}\,|\mathcal{S}_c|^2 \prod_{i=1,2} \frac{1}{\hat{j}_i} \sum_{m_i} \langle \phi^{m_i}_{j_i} | (1 - |\mathcal{S}_i|^2) | \phi^{m_i}_{j_i} \rangle \quad (35)$$

and the associated residue longitudinal momentum distribution is

$$\frac{d\sigma^{\rm unc}_{j_1 j_2}}{d\kappa_c} = \int d\kappa_1 \int d\kappa_2\, \delta(\kappa_c + \kappa_1 + \kappa_2) \int d\vec{b} |\mathcal{S}_c(b)|^2 \times \prod_{i=1,2} \frac{1}{\hat{\ell}_i^2} \sum_{\lambda_i} \int ds_i\, s_i \mathcal{H}_{\lambda_i \lambda_i}(i) \left| \mathcal{R}^{j_i}_{\ell_i \lambda_i}(i) \right|^2. \quad (36)$$

This distribution is shown (solid line with open squares) in Fig. 5 and is significantly broader than the correlated $I^\pi = 0^+$ and 2^+ distributions. This demonstrates once again that the I-dependent correlations, built into the differential joint position probabilities $\tilde{\mathcal{P}}_f(\vec{s}_1, \vec{s}_2, \kappa_c)$ of Eq. (18) by the correlated two-nucleon overlaps, are essential to generating the correct longitudinal momentum distributions from Eq. (19).

D. Sensitivity to nucleon separation energy

We consider the degree of sensitivity of the two-nucleon stripping momentum distributions to the two-nucleon separation energy. In one-nucleon knockout it is well-documented that stronger binding leads to more spatially confined wave functions and to broader momentum distributions. Given the importance of pair correlations, as already discussed, the resulting κ_c distributions are less intuitive in two-nucleon removal. The separation energies of well-bound nucleons are typically of the order of 15–20 MeV in cases of recent interest (and in later examples) and were 15 MeV per proton in the ^{28}Mg test case used above. Figure 7 shows correlated

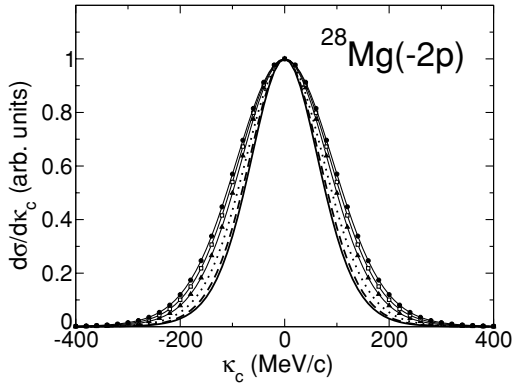

FIG. 7. Calculated $I^\pi = 0^+, \pi[0d_{5/2}]^2$ two-proton stripping longitudinal momentum distributions from ^{28}Mg at 82 MeV/u. The curves result from protons initially bound by 1 (solid), 2, 5, 10, 15, and 20 MeV. All distributions have been normalized to the same peak value.

calculations of the longitudinal momentum distributions for $I^\pi = 0^+, \pi[0d_{5/2}]^2$, two-proton stripping from ^{28}Mg at 82 MeV/u. The $I^\pi = 0^+$ state is chosen because this case maximizes the effects of the two-proton correlations. The curves shown are for protons initially bound by 1, 2, 5, 10, 15, and 20 MeV. The momentum distributions are subtly changed, but are nevertheless relatively insensitive to the proton separation energy, compared, for example, to the changes in the widths of the distributions for the analogous one-nucleon removal reaction over this range of separation energies.

E. Diffraction-stripping contributions

We now consider treatment of the mechanism where one nucleon is diffracted and the other stripped. Calculations of these terms is complicated by the presence of the $\mathcal{K}_3$ (projection) term in the associated diffraction-stripping operator $\mathcal{O}_{\rm ds}$ in Eq. (11). The κ_c distribution due to $\mathcal{K}_2$ alone can be calculated in a way very similar to that for the stripping terms. Calculation of the residue momentum distribution from the $\mathcal{K}_3$ term is less straightforward.

As $\mathcal{O}_{\rm ds}$ is written, there are very large and canceling contributions from the $\mathcal{K}_2$ and $\mathcal{K}_3$ terms and both must be treated carefully to obtain a reliable diffraction-stripping cross section. This was done in Ref. [22]. The source of these cancelations is that, as written, there are large contributions to both terms when the nonabsorbed (diffracted) nucleon is far from the target, and its $\mathcal{S}(b) \to 1$. However, in this region there will be no diffraction as the nucleon does not interact with the target. In fact the diffraction dissociation events require a relatively strong interaction with the target, involving smaller impact parameters (as per Fig. 4).

In the no-recoil approximation we can rewrite the operators $\mathcal{K}_2$ and $\mathcal{K}_3$, replacing $\mathcal{S}_i \to [1 - \mathcal{S}_i]$ for the *diffracted* nucleon only, with (identically) the same exclusive diffraction-stripping partial cross sections $\sigma_{\rm ds}^{(f)}$. We call these transformed operators $\bar{\mathcal{K}}_2$ and $\bar{\mathcal{K}}_3$. So, for example,

$$\bar{\mathcal{K}}_2(1,2) = |1-\mathcal{S}_1|^2[1-|\mathcal{S}_2|^2] + [1-|\mathcal{S}_1|^2]|1-\mathcal{S}_2|^2. \quad (37)$$

In this operator form, $(1 - \mathcal{S}_i)$ encompasses the expected surface localization of the diffraction mechanism and removes the long-range cancelations of the original $\mathcal{K}$. The result is that only 15% or less of the diffraction-stripping cross section is now associated with the $\bar{\mathcal{K}}_3$ term, which we neglect for the purposes of the diffraction-stripping momentum distribution calculation. Upon defining the additional, modified φ_i integral

$$\bar{\mathcal{H}}_{\lambda\lambda'}(i) = \int_0^{2\pi} d\varphi_i |1-\mathcal{S}_i(b_i)|^2 \exp[i\varphi_i(\lambda-\lambda')], \quad (38)$$

our diffraction-stripping $d\sigma_{\rm ds}^{(f)}/d\kappa_c$ are also given by Eq. (32) but where the *direct* and *exchange* terms are now

$$\begin{aligned}
\text{direct} = {} & \mathcal{G}^{\beta_1\beta_2\beta_1'\beta_2' I}_{\lambda_1\lambda_2\lambda_1'\lambda_2'} \big\{ \big[\bar{\mathcal{H}}_{\lambda_1\lambda_1'}(1)\mathcal{H}_{\lambda_2\lambda_2'}(2) + \mathcal{H}_{\lambda_1\lambda_1'}(1)\bar{\mathcal{H}}_{\lambda_2\lambda_2'}(2)\big] \\
& \times \mathcal{R}^{j_1}_{\ell_1\lambda_1}(1)\mathcal{R}^{*j_1'}_{\ell_1'\lambda_1'}(1)\mathcal{R}^{j_2}_{\ell_2\lambda_2}(2)\,\mathcal{R}^{*j_2'}_{\ell_2'\lambda_2'}(2) \\
& + \big[\bar{\mathcal{H}}_{\lambda_1\lambda_1'}(2)\mathcal{H}_{\lambda_2\lambda_2'}(1) + \mathcal{H}_{\lambda_1\lambda_1'}(2)\bar{\mathcal{H}}_{\lambda_2\lambda_2'}(1)\big] \\
& \times \mathcal{R}^{j_1}_{\ell_1\lambda_1}(2)\mathcal{R}^{*j_1'}_{\ell_1'\lambda_1'}(2)\mathcal{R}^{j_2}_{\ell_2\lambda_2}(1)\mathcal{R}^{*j_2'}_{\ell_2'\lambda_2'}(1)\big\} \\
\text{exchange} = {} & (-)^{j_1+j_2-I}\mathcal{G}^{\beta_2\beta_1\beta_1'\beta_2' I}_{\lambda_2\lambda_1\lambda_1'\lambda_2'} \big\{ \big[\bar{\mathcal{H}}_{\lambda_2\lambda_1'}(1)\mathcal{H}_{\lambda_1\lambda_2'}(2) \\
& + \mathcal{H}_{\lambda_2\lambda_1'}(1)\bar{\mathcal{H}}_{\lambda_1\lambda_2'}(2)\big]\mathcal{R}^{j_2}_{\ell_2\lambda_2}(1)\mathcal{R}^{*j_1'}_{\ell_1'\lambda_1'}(1)\mathcal{R}^{j_1}_{\ell_1\lambda_1}(2) \\
& \times \mathcal{R}^{*j_2'}_{\ell_2'\lambda_2'}(2) + \big[\bar{\mathcal{H}}_{\lambda_2\lambda_1'}(2)\mathcal{H}_{\lambda_1\lambda_2'}(1) \\
& + \mathcal{H}_{\lambda_2\lambda_1'}(2)\bar{\mathcal{H}}_{\lambda_1\lambda_2'}(1)\big]\mathcal{R}^{j_2}_{\ell_2\lambda_2}(2)\mathcal{R}^{*j_1'}_{\ell_1'\lambda_1'}(2) \\
& \times \mathcal{R}^{j_1}_{\ell_1\lambda_1}(1)\mathcal{R}^{*j_2'}_{\ell_2'\lambda_2'}(1)\big\}.
\end{aligned}$$

The resulting momentum distributions are compared to those of the stripping mechanism in Fig. 8 where they are shown to be essentially identical. We reiterate the discussion and very general arguments of Sec. II C. Because the diffraction-stripping and the stripping events sample very similar regions of the two-nucleon overlap, it is to be expected that the two mechanisms find the same momentum content in the two-nucleon wave functions and yield essentially identical longitudinal momentum distributions. Moreover, the strong surface localization shown in Fig. 4 means that the shapes of the $d\sigma^{(f)}/d\kappa_c$ distributions can be estimated reasonably reliably from the two-nucleon overlap only, by calculating the $\bar{\mathcal{P}}_f$ of Eq. (18) for fixed nucleon positions at the projectile surface, as was done in Ref. [30].

We note that the $\mathcal{S}_i \to [1 - \mathcal{S}_i]$ substitution used above is even more valuable in simplifying the calculation of diffraction dissociation contributions to one-nucleon knockout reactions. In the present application, the necessity for a second nucleon to be absorbed introduces a natural cutoff of the integral over b; there is no such cutoff in the one-nucleon knockout case. As here, the momentum distributions from the diffraction dissociation and stripping mechanisms are found to be essentially identical in that case also.

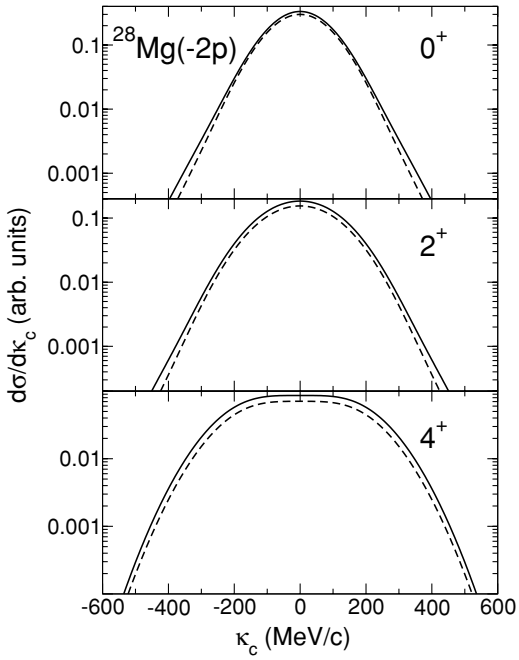

FIG. 8. Comparison of the calculated longitudinal momentum distributions from the diffraction-stripping (dashed) and the stripping (solid) mechanisms for $\pi[0d_{5/2}]^2$ two-proton removal from ^{28}Mg at 82 MeV/u. Curves are for the $I^\pi = 0^+$ (top), 2^+ (middle) and 4^+ (bottom) final states.

IV. APPLICATION TO TWO-PROTON AND TWO-NEUTRON KNOCKOUT REACTIONS

A. Reaction and structure inputs

Here we identify some outstanding details of inputs to the reaction calculations. In all cases the structure inputs, the two-nucleon overlaps information, were taken from the shell model TNA. Details are given or referenced for each example reaction. The required nucleon- and core-target S matrices were calculated from the residue and target neutron and proton single-particle densities and an effective nucleon-nucleon interaction, as was discussed in detail in Ref. [33]. The core densities used were taken from spherical Hartree-Fock calculations, using the SkX Skyrme interaction [34], and the ^{9}Be target density was described by a single Gaussian of root-mean-squared radius 2.36 fm.

The removed-nucleon bound-state wave functions were calculated in Woods-Saxon wells with geometry parameters chosen to fit the root-mean-squared radii of the corresponding single-particle orbitals obtained from the spherical (SkX interaction) Hartree-Fock calculations. This procedure was also discussed in detail in Ref. [33]. A spin-orbit potential, with a depth of 6 MeV, and with the same geometry as the fitted Woods-Saxon wells, was used in all cases. The ground-state to ground-state two-nucleon separation energies were taken from the 2003 mass evaluation [35]. The two removed nucleons were assumed to be equally bound. For transitions to excited final states the effective two-nucleon separation energies were increased by the excitation energy of the final state in question, the two nucleons still being assumed to be equally bound.

V. COMPARISONS WITH EXPERIMENT

Here we consider three specific applications of the developed formalism to confront recent measurements of two-like-nucleon knockout residue longitudinal momentum distributions made at the National Superconducting Cyclotron Laboratory at Michigan State University. In these specific applications, to ^{22,28}Mg and ^{38}Si secondary beams, the two-nucleon configurations in the projectile ground states and their TNA were taken from the already published analyses of the associated partial cross section data in Refs. [22,36], and [26], respectively. We consider quantitatively the residue longitudinal momentum distributions of the reactions ^{9}Be (^{28}Mg,^{26}Ne)X, ^{9}Be (^{22}Mg, ^{20}Mg)X, and ^{9}Be (^{38}Si,^{36}Mg)X at midtarget energies of 82, 75, and 83 MeV/u.

All of these measurements used event-by-event trajectory reconstruction using the large-acceptance S800 spectrograph [37]. The neutron-rich and neutron-deficient projectiles were produced by projectile fragmentation. The particle identification in the entrance and exit channels, details of the associated experimental setups, and the magnitudes of the measured cross sections are described in Refs. [20,26,36]. Theoretical cross sections for the ^{28}Mg and ^{38}Si projectile cases are discussed in Refs. [22] and [26]. The momentum widths of the incoming ^{22,28}Mg and ^{38}Si beams were restricted to 0.5, 0.5, and 1.66%, respectively. The momentum profiles of the unreacted beams passing through the target were also measured in the spectrograph.

The location of the reaction vertex inside the target is of course unknown, which introduces an additional momentum spread due to the differential energy loss of residues produced near the front or the back of the reaction target. This effect was negligible for the two-neutron removal reaction and was strongest for the two-proton removal from ^{38}Si to ^{36}Mg, where $\delta p = 0.29$ GeV/c. The theoretical (projectile rest frame) longitudinal momentum distributions discussed here must, therefore, be corrected for: (a) relativistic broadening in the boost to the laboratory frame, (b) convoluted with the finite momentum profiles of the unreacted beams, and (c) corrected for the differential energy loss in the reaction target, prior to their comparison with these measured data sets.

Gamma-ray spectroscopy was performed in all of the reported measurements and allowed the identification of the residue final states. Full details, including the γ-ray spectra, can be found in Refs. [20,26,36]. For the ^{20,36}Mg residues, the relative population of the 0^+ ground and 2^+ first excited states—the only states populated—were determined from the γ-ray yields in coincidence with the residue. Detailed consideration has been given to the knockout reaction cross sections in Refs. [22,26,36], based on the reaction methodology used here. Our new interest here is comparisons with the predicted shapes of the longitudinal momentum distributions.

A. Two-neutron knockout from ^{22}Mg

The removal of two neutrons from neutron-deficient ^{22}Mg has been studied previously [36]. Two final states were observed, being the $J^\pi_f = 0^+$ ground state and first 2^+ excited

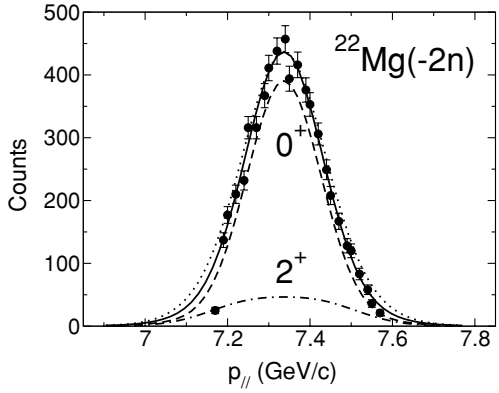

FIG. 9. Theoretical inclusive longitudinal momentum distributions (solid) with the 0^+ (dashed) and 2^+ (dash-dot) components. All curves have Lorentz boost and beam profile adjustments applied. The 0^+ and 2^+ distributions have been scaled to match the experimental γ-ray branching ratios of 84 and 16%, respectively. Applying the theoretical (shell model) branching ratios (of 64 and 36%) gives the dotted curve, normalized to the same peak value, which is slightly broader than the experimental distribution off-peak.

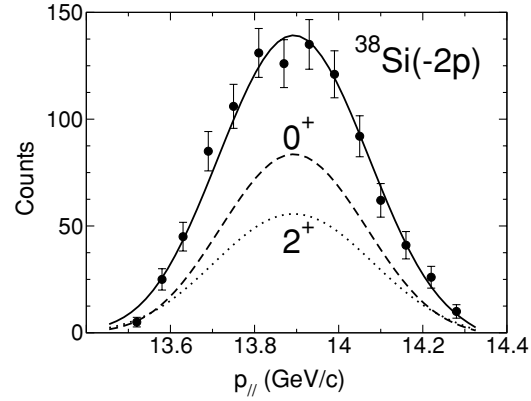

FIG. 10. Measured (symbols) and theoretical (solid curves) inclusive momentum distributions of ^{36}Mg residues after two-proton knockout from ^{38}Si at 83 MeV/u. The theoretical curves for the 0^+ (dashed) and 2^+ (dotted) states are weighted according to the γ-ray data, being 58 and 42%, respectively. All calculations take account of the beam profile and differential momentum loss in the target.

state. The incident beam had a narrow momentum resolution of 0.5%, which was essentially the only experimental broadening.

Because the two-neutron removal reaction does not change the charge of the projectile, the differential energy loss broadening is minimal and the experimental distribution, dominated by the 0^+ ground state transition, is very narrow, as is predicted theoretically. The branching ratios, determined from the γ-ray spectroscopy, were 84 and 16%, respectively. The shell model calculations underestimate the 0^+ branching ratio, giving 64 and 36%. Figure 9 shows the calculated ^{22}Mg residue longitudinal momentum distributions. The figure also shows the longitudinal momentum distributions using the experimental and shell model branching ratios. The narrow, theoretically predicted 0^+ pair removal momentum distribution is beautifully confirmed by this data set.

B. Two-proton knockout from ^{38}Si

The removal of two protons from ^{38}Si, populating states in ^{36}Mg, was discussed previously in Ref. [26], where the TNA were taken from shell model calculations using the *sd*-shell model space ($0\hbar\omega$) and the SDPF-M effective interaction. Two final states were observed experimentally, the $J_f^\pi = 0^+$ ground state and first excited 2^+ state. Because the ^{38}Si ground state is well described by $0\hbar\omega$ configurations, the direct two-proton knockout reaction can populate only the $0\hbar\omega$ components of the ^{36}Mg wave functions, which are expected to contain strong $2\hbar\omega$ intruder components. The ratio of the experimental and theoretical cross sections thus indicates the proportion of $0\hbar\omega$ (and hence $2\hbar\omega$) components in the ^{36}Mg ground state and first excited 2^+ state.

The incident beam had a wide momentum resolution of 1.66%, which generates significant broadening (see Fig. 10). The figure shows the shapes of the calculated momentum distributions. These are scaled to match the experimental (inclusive) cross section with the 0^+ and 2^+ state components weighted by 58 and 42%, in accord with the γ-ray data. The theoretical distributions are strongly broadened, but the agreement with the experimental data is excellent.

C. Two-proton knockout from ^{28}Mg

The inclusive and exclusive cross sections for the removal of two well-bound protons from ^{28}Mg have been discussed previously [20–22]. Four ^{26}Ne final states were observed, being the $J_f^\pi = 0^+$ ground state, the first and second 2^+ excited states, and the first 4^+ state. The TNA are tabulated in Ref. [21], calculated using the *sd*-shell model space and the USD interaction.

Since the publication of Ref. [20], the inclusive data have been reanalyzed and exclusive longitudinal distributions for the $J_f^\pi = 0^+$ ground state and 4_1^+ excited state have been extracted. These experimental exclusive momentum distributions were obtained in a manner similar to that of previous work on one-nucleon knockout exclusive cross sections [10]. The ^{26}Ne 4^+ distribution was obtained by gating on the 4^+ to 2^+ γ-ray transition, observed at 1.48 MeV, in coincidence with the ^{26}Ne residues. The limited statistics are a direct consequence of the efficiency of the Segmented Germanium Array (SeGA) [38] used to detect the γ rays. The ^{26}Ne ground state longitudinal momentum distribution was obtained by subtracting the distributions in coincidence with the two γ-ray transitions observed in the data set at 1.48 and 2.02 MeV (2^+ to 0^+) from the inclusive distribution, after taking into account the γ-ray photo-peak detection efficiencies at these two energies. All longitudinal momentum distributions (including the inclusive) were reconstructed from several rigidity settings of the S800 spectrograph, to cover their full range as much as possible. The low statistics at the low longitudinal momenta is due to a smaller exposure time at the low momentum setting.

The experimental distributions and fully correlated calculations are shown in Fig. 11. Despite the significant broadening of the theoretical distributions due to experimental resolutions, the agreements with the data are very good.

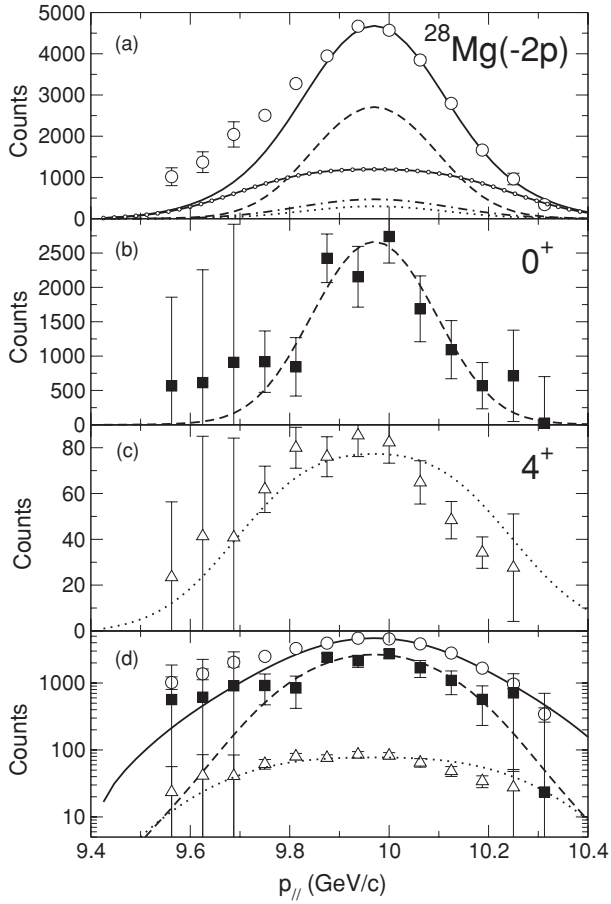

FIG. 11. Measured (symbols) and theoretical (curves) inclusive and exclusive longitudinal momentum distributions after two-proton knockout from ^{28}Mg at 82 MeV/u. Panel (a) shows the measured inclusive distribution and that constructed from the weighted 0^+, 2^+_1, 4^+_1, and 2^+_2 distributions [22]. Panel (b) shows the ^{26}Ne(0^+, g.s.) distribution, panel (c) the ^{26}Ne(4^+_1, 3.50 MeV) final state distribution, and panel (d) shows all distributions on a logarithmic scale. All the calculated shapes take account of the beam profile (0.1 GeV/c) and differential energy loss in the target (0.24 GeV/c) broadening.

D. Heavy nuclei: Two-proton knockout from ^{208}Pb

The three chosen experimental examples above describe two-nucleon knockout from sd-shell single-particle states. It is of interest to consider the (theoretical) momentum distributions resulting from the removal of two protons from heavier nuclei, such as ^{208}Pb. In this case, the number of active orbitals is larger, covering $\pi[2s_{1/2}]$ to $\pi[0h_{11/2}]$. This allows (i) study of the expected sensitivity to the orbital angular momentum of the removed nucleons, (ii) examination of the momentum distributions for high spin states, and (iii) consideration of the magnitude of the effects on the shapes of knockout momentum distributions from heavier mass projectiles. Calculations were performed at 500 MeV/u on a ^{9}Be target. Concerning the last point, we might expect that, as the projectile becomes larger and the rms radii of the nucleon single-particle wave functions increase, the resulting momentum distributions may become more narrow.

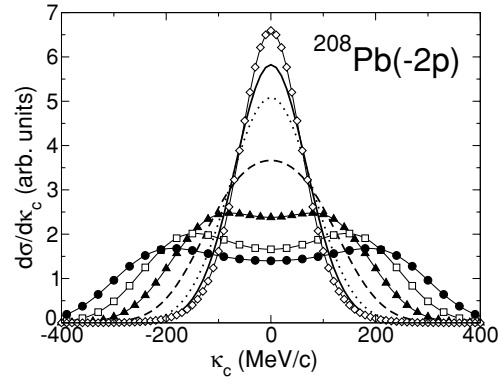

FIG. 12. Heavy residue longitudinal momentum distributions after $\pi[0h_{11/2}]^2$ two-proton knockout from ^{208}Pb for $I^\pi = 0^+$ (solid), 2^+ (dotted), 4^+ (dashed), 6^+ (solid triangles), 8^+ (open squares), and 10^+ (solid circles). The distribution for $I^\pi = 0^+, \pi[2s_{1/2}]^2$ two-proton knockout is also shown (solid line with open diamonds). The difference in the 0^+ distributions for $\pi[0h_{11/2}]^2$ and $\pi[2s_{1/2}]^2$ knockout is relatively small when compared to the changes when I is increased.

We have already seen that increasing the total angular momentum of the knocked-out nucleon pair from the initial state, from 0 to 4 in the case of ^{28}Mg, led to distinctly wider longitudinal momentum distributions. In a $\pi[0h_{11/2}]^2$ two-proton removal from ^{208}Pb we can populate simple low-seniority states with spins from $J^\pi_f = 0^+$ to 10^+. These theoretical momentum distributions are shown in Fig. 12. The distribution for $J^\pi_f = 0^+, \pi[2s_{1/2}]^2$ two-proton knockout is also shown (solid line with open diamonds). As demonstrated earlier, we also anticipate large differences in the momentum distributions for each final magnetic substate. This is shown in Fig. 13.

As has been discussed for one-nucleon knockout, e.g., Ref. [3], cuts in the heavy residue longitudinal momentum

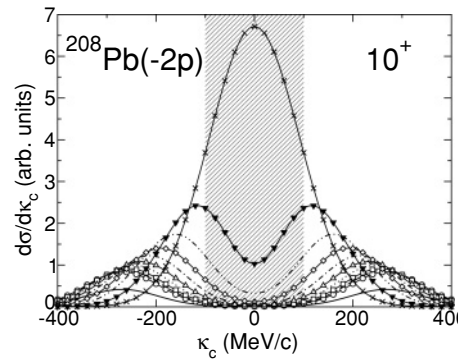

FIG. 13. Heavy residue longitudinal momentum distributions for $\pi[0h_{11/2}]^2$ two-proton knockout from ^{208}Pb with $I^\pi = 10^+$, showing the different magnetic substate distributions. Shown are $|\mu| = 0$ (solid), 1 (open circles), 2 (dashed), 3 (open squares), 4 (dotted), 5 (open triangles), 6 (dot-dashed), 7 (open diamonds), 8 (dot-dot-dashed), 9 (inverted solid triangles), and 10 (crosses). The shaded region shows a possible cut in the heavy residue momentum that would very significantly alter the relative population of the large $|\mu|$ substates.

TABLE I. Fractional populations of different magnetic substates of the heavy residue after the $\pi[0h_{11/2}]^2$,^{208}Pb$(-2p)$ reaction to the $I^\pi = 10^+$ final state. Calculations were performed at 500 MeV/u on a ^{9}Be target. The cut on the momentum distribution between -100 and $+100$ MeV/c significantly enhances the fractional population of the large $|\mu|$ substates.

$\|\mu\|$	Percentage population										
	0	1	2	3	4	5	6	7	8	9	10
Full	2.6	5.3	5.5	5.8	6.3	6.9	7.7	8.8	10.7	14.4	25.8
Cut	0.2	0.4	0.4	0.5	0.7	1.1	1.9	3.4	7.4	19.0	64.9

can lead to significant alignment of the reaction products, providing additional spectroscopic possibilities and the means for further rigorous tests of the reaction mechanisms. It is also interesting to note the fraction of each magnetic substate populated. As an example, we have calculated the fractional population of substates with $|\mu|$ for the $J_f^\pi = 10^+$ transition, shown in Table I. The fractional populations when the cut shown by the shaded region in Fig. 13 is applied are also tabulated. These indicate that the reaction mechanism, particularly for large-spin final states, leads to significant population of the stretched-state configurations, particularly if restrictions are placed on the longitudinal momenta of the residues.

These calculations show that the observations made in this work, and tested empirically here for nuclei with masses $A < 40$, persist to higher energies and heavy nuclei. The information available through the momentum distributions is potentially considerable, providing clear spectroscopic signals. We have shown that momentum distribution calculations are robust and driven by simple considerations, such as the reaction geometry and its surface dominance.

VI. SUMMARY

We have formulated theoretical calculations of final-state exclusive longitudinal momentum distributions of projectile residues after fast, direct two-nucleon knockout. Both the stripping and the diffraction-stripping removal mechanisms were considered and were shown to result in essentially identical residue distributions. The sensitivity of these distributions has been investigated. We have shown that the total angular momentum carried by the two nucleons when removed from the initial state, the spin of the final state for an even-even projectile, is the primary factor in determining the shape and width of the resulting longitudinal momentum distribution. This result has high spectroscopic value for determining the spins of states of rare nuclei. There was a much weaker sensitivity to nucleon separation energy and the individual angular momenta of the removed nucleons, as was shown by the similarity of the distribution for the 0^+ state in ^{206}Hg from $\pi[0h_{11/2}]^2$ and $\pi[2s_{1/2}]^2$ two-proton knockout from ^{208}Pb. It has been confirmed that the use of correlated two-nucleon wave functions is essential to generate the widths of experimentally observed distributions.

Application of the methodology to three available measurements has provided detailed confirmation of these theoretical expectations. Further dedicated measurements of exclusive momentum distributions of two-neutron knockout from even-even projectiles will provide the most rigorous test of the ideas presented here. Our conclusion is that exclusive two-nucleon knockout parallel momentum distribution measurements have high spectroscopic potential for use in studies of the spins and structure of states in rare nuclei.

ACKNOWLEDGMENTS

We thank Professor B. Alex Brown for his continued advice with the shell model input and its interpretation. This work was supported by the United Kingdom Science and Technology Facilities Council (STFC) under Grants ST/F012012 and EP/D003628 and by the US National Science Foundation under Grants PHY-0606007, PHY-0555366, and PHY-0758099. A.G. is supported by an Alfred P. Sloan Research Grant.

[1] H. Esbensen, Phys. Rev. C **53**, 2007 (1996).
[2] E. Sauvan *et al.*, Phys. Lett. **B491**, 1 (2000); Phys. Rev. C **69**, 044603 (2004).
[3] P. G. Hansen and J. A. Tostevin, Annu. Rev. Nucl. Part. Sci. **53**, 219 (2003).
[4] D. Cortina-Gil *et al.*, Phys. Lett. **B529**, 36 (2002).
[5] A. Navin *et al.*, Phys. Rev. Lett. **81**, 5089 (1998).
[6] J. A. Tostevin, J. Phys. G: Nucl. Part. Phys. **25**, 735 (1999).
[7] A. Navin *et al.*, Phys. Rev. Lett. **85**, 266 (2000).
[8] T. Aumann *et al.*, Phys. Rev. Lett. **84**, 35 (2000).
[9] V. Guimarães *et al.*, Phys. Rev. C **61**, 064609 (2000).
[10] V. Maddalena *et al.*, Phys. Rev. C **63**, 024613 (2001).
[11] J. Enders *et al.*, Phys. Rev. C **65**, 034318 (2002).
[12] B. A. Brown, P. G. Hansen, B. M. Sherrill, and J. A. Tostevin, Phys. Rev. C **65**, 061601(R) (2002).
[13] A. Gade *et al.*, Phys. Rev. C **69**, 034311 (2004).
[14] A. Gade *et al.*, Phys. Rev. Lett. **93**, 042501 (2004).
[15] J. R. Terry *et al.*, Phys. Rev. C **69**, 054306 (2004).
[16] A. Gade *et al.*, Phys. Rev. C **71**, 051301(R) (2005).
[17] J. R. Terry *et al.*, Phys. Lett. **B640**, 86 (2006).
[18] A. Gade *et al.*, Phys. Rev. C **74**, 047302 (2006).
[19] L. A. Riley *et al.*, Phys. Rev. C **78**, 011303(R) (2008).
[20] D. Bazin *et al.*, Phys. Rev. Lett. **91**, 012501 (2003).
[21] J. A. Tostevin, G. Podolyák, B. A. Brown, and P. G. Hansen, Phys. Rev. C **70**, 064602 (2004).
[22] J. A. Tostevin and B. A. Brown, Phys. Rev. C **74**, 064604 (2006).
[23] K. Yoneda *et al.*, Phys. Rev. C **74**, 021303(R) (2006).
[24] J. Fridmann *et al.*, Phys. Rev. C **74**, 034313 (2006).
[25] A. Gade *et al.*, Phys. Rev. C **74**, 021302(R) (2006).
[26] A. Gade *et al.*, Phys. Rev. Lett. **99**, 072502 (2007).
[27] B. Bastin *et al.*, Phys. Rev. Lett. **99**, 022503 (2007).
[28] P. Adrich *et al.*, Phys. Rev. C **77**, 054306 (2008).
[29] J. A. Tostevin, J. Phys. Conf. Ser. **49**, 21 (2006).
[30] J. A. Tostevin, Eur. Phys. J. Spec. Top. **150**, 67 (2007).
[31] E. C. Simpson, J. A. Tostevin, D. Bazin, B. A. Brown, and A. Gade, Phys. Rev. Lett. **102**, 132502 (2009).

[32] D. M. Brink and G. R. Satchler, *Angular Momentum* (Oxford University Press, London, 1993), 3rd edition.
[33] A. Gade *et al.*, Phys. Rev. C **77**, 044306 (2008).
[34] B. A. Brown, Phys. Rev. C **58**, 220 (1998).
[35] G. Audi, A. H. Wapstra, and C. Thibault, Nucl. Phys. **A729**, 337 (2003).
[36] A. Gade *et al.*, Phys. Rev. C **76**, 024317 (2007).
[37] D. Bazin, J. A. Caggiano, B. M. Sherrill, J. Yurkon, and Z. Zeller, Nucl. Instrum. Methods Phys. Res. B **204**, 629 (2003).
[38] W. F. Mueller, J. A. Church, T. Glasmacher, D. Gutknecht, G. Hackman, P. G. Hanse, Z. Hu, K. L. Miller, and P. Quirin, Nucl. Instrum. Methods Phys. Res. A **466**, 492 (2001).